ACS OMEGA

http://pubs.acs.org/journal/acsodf

Article

Highly NH_3 Sensitive and Selective $Ti_3C_2O_2$-Based Gas Sensors: A Density Functional Theory-NEGF Study

Kaiyi Weng, Jiahe Peng, Zuhao Shi, Arramel Arramel, and Neng Li*

Cite This: *ACS Omega* 2023, 8, 4261−4269

Read Online

ACCESS | Metrics & More | Article Recommendations | Supporting Information

ABSTRACT: Ammonia (NH_3) detection at the early stage is an important precaution for human health and agricultural production. However, conventional sensing materials are difficult to achieve all the targeted operational performances such as low power consumption and high selectivity. MXenes are a type of graphene-like emergent material equipped with abundant surface sites benefiting gas-sensing applications. In the work, we discuss the sensing performance of $Ti_3C_2O_2$ to anticipate harmful and polluting NH_3 gases by density functional theory and nonequilibrium Green's function. The adsorption geometry, charge difference density, and partial density of states are discussed to understand the nature of interactions between gas molecules and $Ti_3C_2O_2$. The theoretical results show that only NH_3 adsorbs onto the nanosheet through chemisorption. Then, a two-electrode $Ti_3C_2O_2$-based gas sensor device is built to unravel the transport properties. Current under different bias voltages indicates the $Ti_3C_2O_2$-based sensor could maintain extremely high sensitivity, demonstrating that $Ti_3C_2O_2$ has great potential for the NH_3 sensor with high selectivity, excellent sensitivity, and low energy consumption. Upon external electric fields, the adsorption energy and charge transfer can be tuned effectively, suggesting that $Ti_3C_2O_2$ is a versatile agent as an ammonia-sensing material.

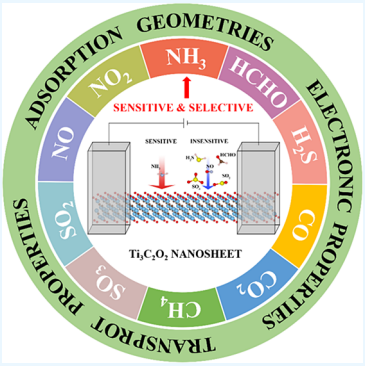

INTRODUCTION

Ammonia is a colorless, water-soluble gas with strong pungent odors. When NH_3 is combined with particulate matter in the atmosphere, the formation of ammonium salts and haze particulate matter will accelerate causing acidification of the ecosystem and eutrophication of water. Moreover, ammonia is harmful to the human body. Therefore, it is vital to detect the presence of ammonia in the ambient environment. Gas sensors are devices capturing environmental changes and output readable signals by postprocessing. In practice, the physical function gas sensors should possess depend on specific purposes and service environments. However, among all the requirements, sensing performance-related ones (sensitivity, selectivity, and rate of response) and reliability-related ones (drift, stability, and interfering gases) are of importance.[1−3] Diverse classes of materials such as semiconducting metal oxides,[4−7] carbon nanotubes,[8,9] and conducting polymers[10,11] are used in research and application of gas sensing. However, achieving the ideal combination of high sensitivity, low cost, and wide operating temperate is still challenging. For example, nanotubes possess great sensitivity but are difficult to manufacture and require a long recovery time.[8] Metal oxide-based gas sensors are low cost but have poor selectivity and require high operating temperature due to the wide band gap and their sensing mechanics.[12,13]

In recent years, MXenes have attracted the attention of worldwide scientists owing to their graphene-like structure. They can be obtained by etching A layers from the MAX phase. The general formula of MXenes is $M_{n+1}X_nT_x$, where M, X, T, and A stand for early transition metal, carbon or/and nitrogen, the functional group obtained during the preparation process, and IIIA or IVA elements, respectively. $Ti_3C_2T_x$ is the first MXene to be discovered and widely investigated throughout their early discoveries.[14] Several superior chemical and physical properties such as good conductivity, large specific surface area, high stability, highly adjustable metal composition, and surface functional groups made $Ti_3C_2T_x$ an excellent material in supercapacitors,[15−17] catalysis,[18−20] optoelectronic devices,[21,22] water purification,[23,24] and gas sensors.[25,26]

In this paper, we explore the possibility of Ti_3C_2 covered with different functional groups (−O, −OH, −F, −Cl) as an ammonia sensor by DFT-NEGF. Here, we assess the respective sensing performances by investigating their interactions with toxic and greenhouse gases. We take CO, CO_2, CH_4, HCHO, H_2S, SO_2, SO_3, NO_2, NO, and NH_3 gases into consideration. Based on the analysis of electronic structures like adsorption geometry, charge density difference, and partial density of states, we find moderate adsorption energy and charge transfer amount of NH_3 on $Ti_3C_2O_2$, verifying the

Received: November 22, 2022
Accepted: January 6, 2023
Published: January 19, 2023

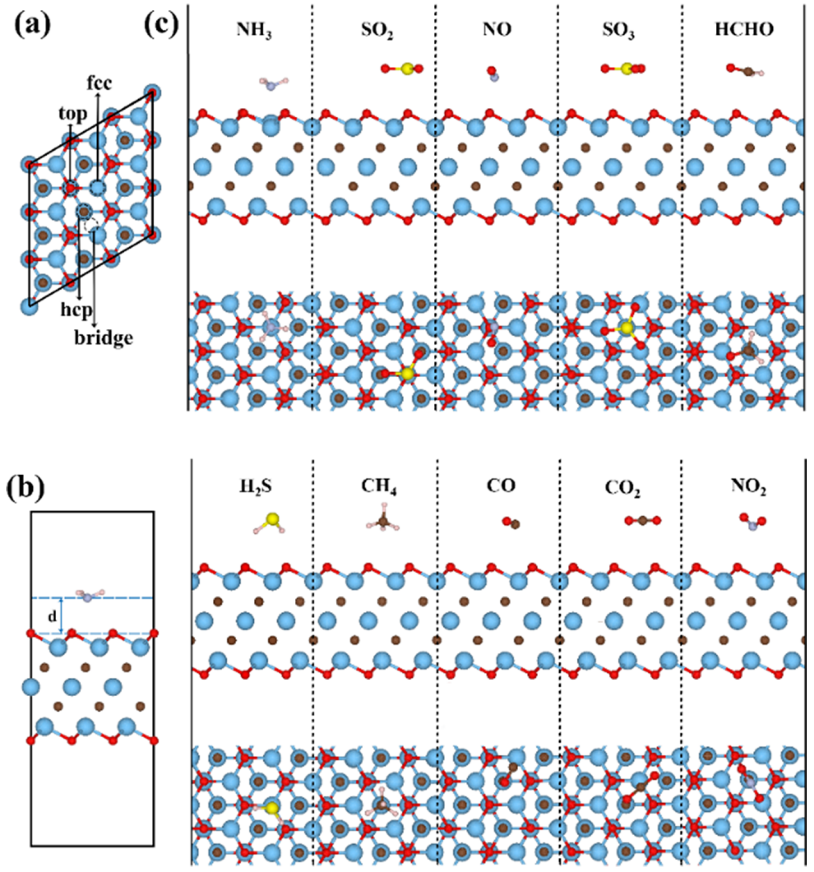

Figure 1. A schematic illustration of $Ti_3C_2O_2$ surface and gas adsorption. (a) Adsorption sites on $Ti_3C_2O_2$, (b) distance between gas and $Ti_3C_2O_2$, and (c) side and top views of gas adsorption configuration. Red: O, blue: Ti; brown: C; white: H, yellow: S, purple: N.

selectivity and sensitivity of $Ti_3C_2O_2$ toward NH_3. Furthermore, the transport properties of $Ti_3C_2O_2$ under bias voltages ranging from 0 to 1 V are evaluated. The dramatic current change of $Ti_3C_2O_2$ with NH_3 adsorption shows $Ti_3C_2O_2$ is a very promising ammonia sensor material. The satisfactory results show the adsorption strength can be tuned effectively by applying external electric fields and offer an effective way to realize the capture and release of ammonia.

COMPUTATIONAL METHODS

The density functional theory (DFT) was used in structural optimizations and performance analyses by Vienna Ab Initio Simulation Package (VASP).[27] Projector augmented wave (PAW) pseudopotentials[28] are used to describe the electron−ion interaction. For the exchange and correlation functionals, we use the Perdew−Burke−Ernzerhof method from the generalized gradient approximation (GGA-PBE).[28] A 15 Å vacuum region was added along the *Z*-direction and a 3 × 3 × 1 supercell structural model was built to eliminate the interaction between adjacent layers and gas molecules, respectively. The *K*-point was set as 5 × 5 × 1, and the cutoff energy for wave function expansion was 500 eV. Meanwhile, the energy and force convergence criteria were less than 10^{-5} eV and 0.01 eV/Å, respectively. The van der Waals interactions between MXenes and gas were described by empirical dispersion correction (DFT-D3).[29]

The adsorption energy (E_{ad}) is defined as follows:

$$E_{ad} = E_{Ti_3C_2T_x+gas} - E_{Ti_3C_2T_x} - E_{gas}$$

where $E_{Ti_3C_2T_x+gas}$ is the total energy of $Ti_3C_2T_x$ with adsorbate, $E_{Ti_3C_2T_x}$ and E_{gas} are the energy of pure $Ti_3C_2T_x$ and isolated gas molecule.

The electron transport calculations were performed by first principles package NANODCAL based on the density functional theory and nonequilibrium Green's function (NEGF-DFT) method.[30] The GGA-PBE and double-zeta polarized (DZP) basis sets were used in these calculations. A larger vacuum slab (20 Å) and three atomic layers along the transport direction in each side (Figure S1) were applied to ensure the potential along the transport direction is smooth. The cutoff energy and *K*-point for devices and electrodes were 80 Hartree, 1 × 8 × 1, and 100 × 6 × 1, respectively.

The current *I* at bias voltage V_b can be obtained using the Landauer−Butiker formula:[31]

$$I = \int_{-\infty}^{+\infty} T(E, V_b)[f_L(E - u_L) - f_R(E - u_R)]dE$$

$$V_b = u_L - u_R$$

where $T(E, V_b)$ is the transmission coefficient, *f* and *u* refer to the Fermi−Dirac distribution function and electrochemical potential, respectively, the subscript *L*/*R* is used to distinguish the left/right electrode.

The sensitivity *S* of the gas sensor is defined as:[32]

$$S = \frac{|I_0 - I|}{I}$$

https://doi.org/10.1021/acsomega.2c07492
ACS Omega 2023, 8, 4261−4269

where I_0 is the current of the clean device and I represents the current of the device with different gas molecules.

The optimized geometric conditions of Ti_3C_2 with functional groups are predetermined to be perpendicular with respect to the middle layer Ti atoms that are considered as the most stable structure.[33−35] Therefore, the sequence calculations discussed in this study are based on these approaches. The $Ti_3C_2T_x$ surfaces and gas adsorption sites are shown in Figures 1a and S2.

RESULTS AND DISCUSSION

The possible adsorption sites and orientations like vertical and horizontal directions of CO, CO_2, CH_4, HCHO, SO_2, SO_3, H_2S, NO_2, NO, and NH_3 on $Ti_3C_2O_2$ are considered. The corresponding adsorption energy, charge transfer amount, and adsorption distance (schematic diagram shown in Figure 1b) of the most stable configurations are summarized in Table 1 and Tables S1−3.

Table 1. Calculated Adsorption Energy (E_{ad}), Bader Charge (ΔQ) of Different Gas Molecule on the $Ti_3C_2O_2$ Supercell, and Interfacial Spacing ($d_{Ti_3C_2O_2-gas}$) (Positive ΔQ Value Represents Substrate as an Electron Acceptor)

gas molecule	E_{ad} (eV)	$d_{Ti_3C_2O_2-gas}$ (Å)	ΔQ (e)
NH_3	−0.420	1.730	0.181
NO	−0.348	2.300	0.226
SO_3	−0.340	2.875	−0.017
SO_2	−0.285	2.876	−0.013
H_2S	−0.254	2.362	0.024
HCHO	−0.233	2.547	−0.004
CH_4	−0.207	2.536	0.004
CO	−0.162	2.761	0.002
CO_2	−0.201	3.010	−0.007
NO_2	−0.185	2.632	−0.003

The negative sign of adsorption energy indicates that the gas molecules can adsorb on the $Ti_3C_2T_2$ surface spontaneously. According to Yang et al.,[13] a suitable gas-sensing material should capture the target gas by weak chemical interactions or strong physical interactions. Too small adsorption energy and large charge transfer (Table S2) often accompany with the gas molecule adsorptions on $Ti_3C_2(OH)_2$, which lead to bond-breaking reactions and poison the sensor so that the sensor cannot be reused.[36] While for −F and −Cl terminated Ti_3C_2, the small charge transfer and relatively large adsorption energy (Tables S1, S3) after adsorption lead to low sensitivity and long response time,[37] which disadvantage to rapid detection. $Ti_3C_2O_2$ exhibits the best selectivity and moderate adsorption energy and charge transfer to NH_3. Therefore, subsequent analytical calculations are based on $Ti_3C_2O_2$.The most stable adsorption geometries are shown in Figure 1c. Based on these results, we find that all interacting gases can realize spontaneous adsorption and maintain their molecule forms. Interestingly, a local structural deformation appears when NH_3 was adsorbed onto the $Ti_3C_2O_2$ surface.

In detail, the Ti atoms at the close proximity of NH_3 slightly move outward, indicating a strong interaction between NH_3 and $Ti_3C_2O_2$. Meanwhile, the adsorption distance between $Ti_3C_2O_2$ and NH_3 is the smallest compared with the others, and we find that this value is slightly smaller than the sum of the covalent radii of O and N, which suggests that NH_3 gas may adsorb on $Ti_3C_2O_2$ by chemical adsorption. While for other gas adsorptions, the distances between gas and $Ti_3C_2O_2$ are still larger than the sum of their covalent radii, inferring the presence of physical adsorptions between the adsorbent and the gas molecules. It is worth mentioning that CO, CO_2, CH_4, and NO_2 occur with few charge transfer and large adsorption energy, indicating poor interaction between the substrate and the adsorbate, that is, $Ti_3C_2O_2$ cannot detect them effectively. Thus, we choose HCHO, SO_2, SO_3, H_2S, NO, and NH_3 as the target gases for the following research.

To further analyze the charge redistribution of the adsorption systems, the charge density difference was calculated. As shown in Figure 2, NO and NH_3 act as strong

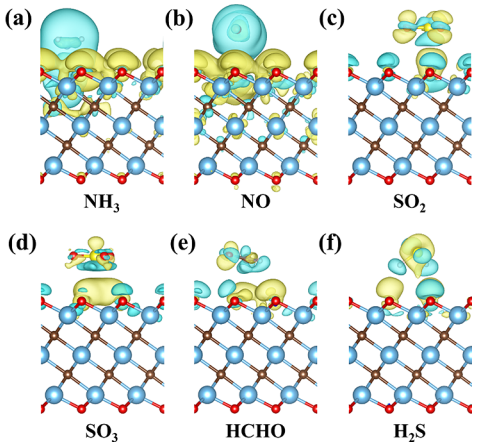

Figure 2. Charge density difference of molecule/$Ti_3C_2O_2$. (a) NH_3/$Ti_3C_2O_2$, (b) NO/$Ti_3C_2O_2$; (c) SO_2/$Ti_3C_2O_2$;(d) SO_3/$Ti_3C_2O_2$; (e) HCHO/$Ti_3C_2O_2$; (f) H_2S/$Ti_3C_2O_2$. Yellow: charge accumulation, cyan: charge depletion. The isosurface value was set to 0.0002 e $Å^{-3}$.

electron donors. Especially, NH_3 overlaps a lot with the $Ti_3C_2O_2$ surface, indicating the existence of a bond between the gas molecule and $Ti_3C_2O_2$. Compared with NH_3 adsorption, the charge density difference of NO/$Ti_3C_2O_2$ is more localized which leads to weaker interaction and no appreciable atomic displacement. In contrast, there are minor charge redistributions between other gas molecules and $Ti_3C_2O_2$, manifesting the $Ti_3C_2O_2$ monolayers capture these gas molecules by physical adsorption.

To analyze the nature of the interactions between gas molecules and $Ti_3C_2O_2$ sheets more intuitively, the partial density of states (PDOS) of the atom with the most charge transfer in each of gas molecule (Figure S3) and the nearby Ti atom and O atom in $Ti_3C_2O_2$ are presented (Figure 3). When the NH_3 adsorbed on the $Ti_3C_2O_2$, the dispersion of N p states overlapped significantly with the d states of Ti and the p states of O from −4 to −1.5 eV, indicating that the N p states are strongly hybridized with the d states of Ti and the p states of O atoms. At the meantime, a slight shift toward E_f was observed in the PDOS of Ti. As for NO/$Ti_3C_2O_2$, the adsorption of NO induced few small peaks of O p states around the Fermi level, demonstrating minute interactions between the N p states and the O p states. However, this character allows more charge transfers between NO and $Ti_3C_2O_2$.[38] For the remaining systems, the PDOS of Ti and O are hardly changed after adsorption, representing that these gases are physically adsorbed on the $Ti_3C_2O_2$ sheets which are consistent with the charge density difference analysis.

https://doi.org/10.1021/acsomega.2c07492
ACS Omega 2023, 8, 4261−4269

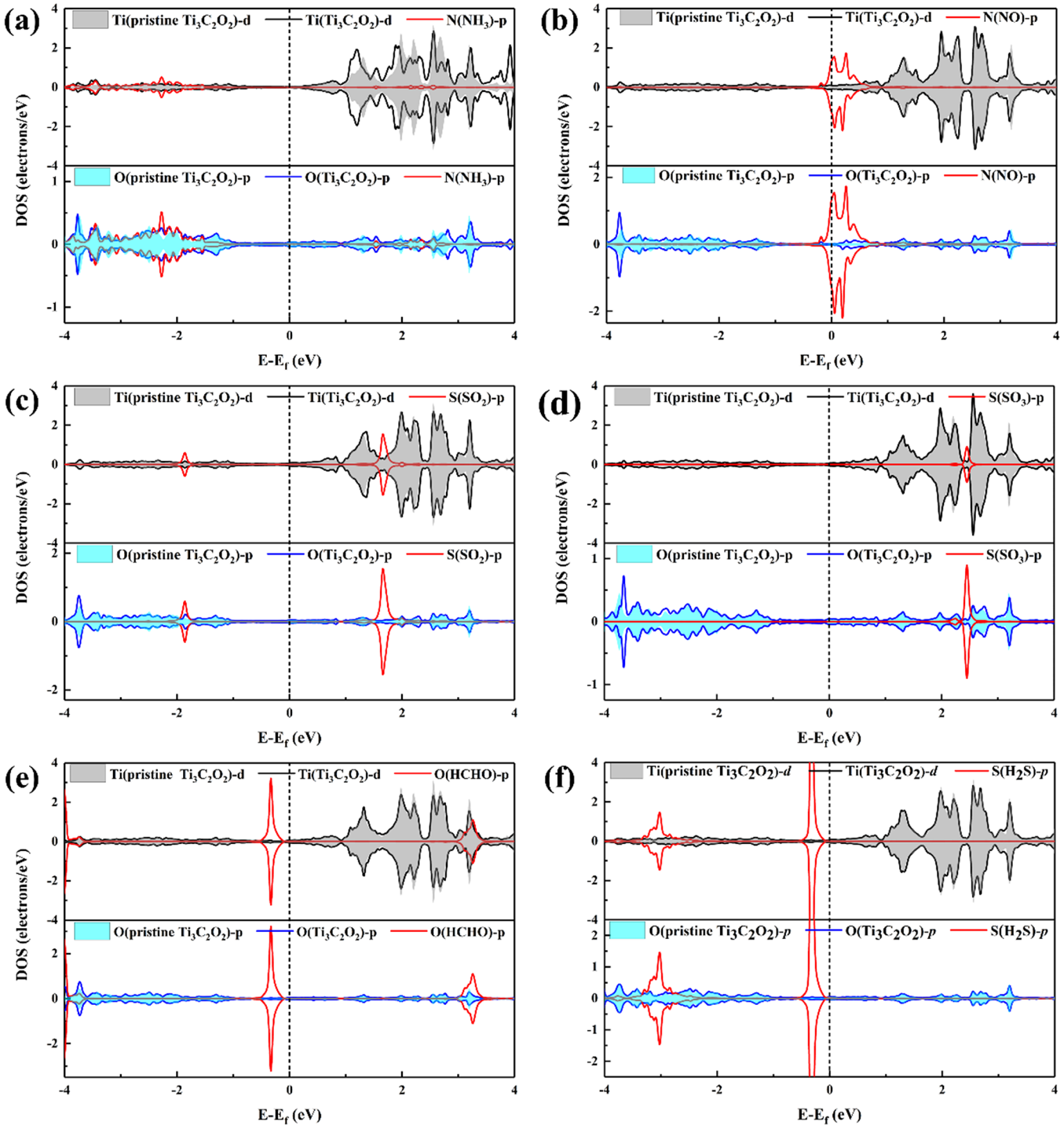

Figure 3. Partial density of states of molecule/$Ti_3C_2O_2$. (a) $NH_3/Ti_3C_2O_2$, (b) $NO/Ti_3C_2O_2$, (c) $SO_2/Ti_3C_2O_2$; (d) $SO_3/Ti_3C_2O_2$;(e) HCHO/$Ti_3C_2O_2$; (f) $H_2S/Ti_3C_2O_2$.

To simulate the electronic transport properties, a $Ti_3C_2O_2$-based sensor consisting of a $Ti_3C_2O_2$ sheet and two $Ti_3C_2O_2$ electrodes is proposed in this investigation. Three atomic layers in each side along the transport direction are added to realize the shielding effect between the central region and the electrodes. Both electrodes and the scattering regions are periodically perpendicular to the transport direction (Figure 4). By applying bias voltages ranging from 0 to 1 V, the current values are depicted in Figure 5a. In general, devices with gases except NH_3 exhibit similar $I-V$ trends with the clean device. After NH_3 adsorption, the device shows a drastic current change, suggesting that $Ti_3C_2O_2$ is a promising ammonia-sensitive material, which is consistent with the experimental results.[25,26]

The device with NH_3 demonstrates a rapid and linear current increment when the bias voltages increase from 0 to 0.4 V, then the current gradually decreases as the voltage increases. In other words, negative differential resistance (NDR) occurs. However, the current value is still about 50% higher than other gas-induced currents. The current increases

https://doi.org/10.1021/acsomega.2c07492
ACS Omega 2023, 8, 4261−4269

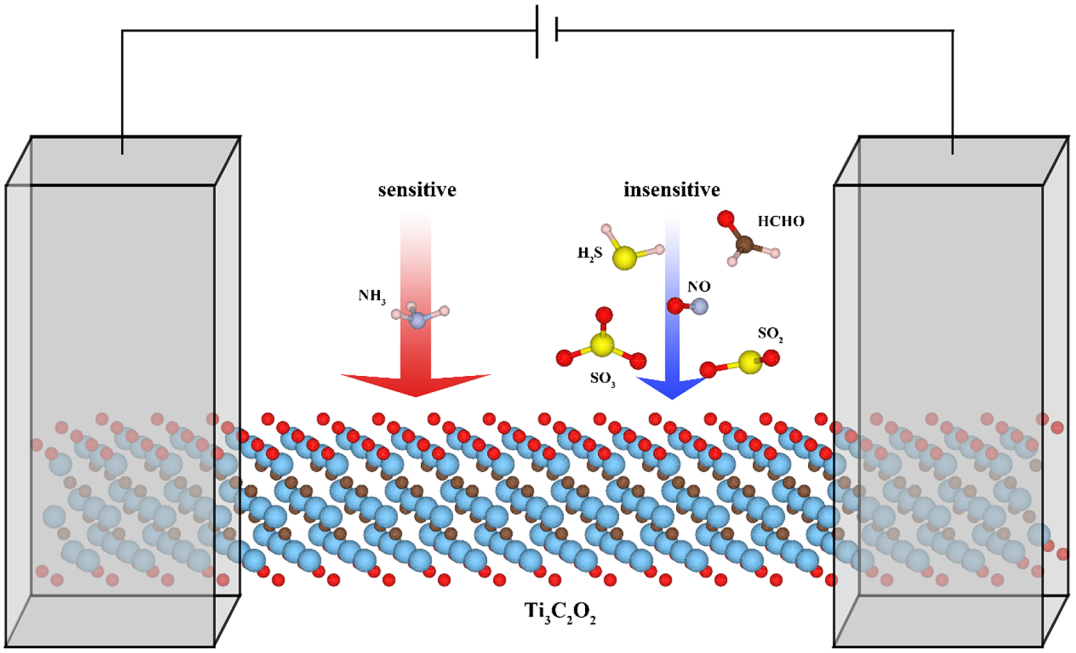

Figure 4. Scheme of the $Ti_3C_2O_2$-based gas sensor. Gray cuboid represents the electrodes. Two distinct downward arrows represent different physical interactions of gases with the $Ti_3C_2O_2$ surfaces.

again when the voltage is continuously increased above 0.8 V, but the slope of the curve is smaller than that at low bias. To describe the current change before and after adsorption quantitatively, we present the sensitivity S of the gas sensor in Figure 5b. For NH_3 adsorption, S could reach 1.8 at V_b = 0.3 V and even the minimum value could reach 0.4. It is worth pointing out that the sensitivity remains higher than 0.8 when the bias voltages are applied ranging from 0.2 to 0.8 V, which shows that $Ti_3C_2O_2$ has a great sensing performance and stability. On the contrary, when SO_2, SO_3, and H_2S adsorb on the surface, the $Ti_3C_2O_2$-based gas sensor is completely insensitive as the values of S are close to 0. The sensitivities to HCHO and NO are slightly higher than the above gases, but the highest value is about 0.2, still much less than that of NH_3, which verifies the sensitivity of $Ti_3C_2O_2$ to NH_3.

Transmission coefficients plotted in Figure 5c,d are calculated to uncover the microscopic mechanisms of the gas sensor. Under different bias voltages, the current is determined by the integral of the transmission coefficient in the bias window. At V_b = 0.1 V, the coefficient of NH_3 near the Fermi level is always higher than that of other gases and clean sensors, indicating more ballistic transports in $NH_3/Ti_3C_2O_2$. At V_b = 1 V, the bias window is from −0.5 to 0.5 eV. Although the coefficient of every system decreases the current still increases due to the expansion of the integration range. Gases except NH_3 show similar coefficient values with the clean device, leading to low sensitivity. While for NH_3, when the energy ranges from −0.5 to about −0.1 eV, the coefficient is the smallest, then it becomes largest and starts to pull away from other gases and lead to the highest current than the other systems.

To figure out the physical origin of NDR, we plotted the transmission spectrum mapping under different bias is illustrated in Figure 6a. The black lines represent different bias windows under different V_b. When the initial voltage increases, a peak gradually shifts into the bias window, making the current increase rapidly. Then, the peak changes its course and gradually moves away. Most of the coefficients in the bias window are close to zero. Consequently, the current is dramatically reduced. To further understand the microscopic image, scattering states are also analyzed. In this work, the scattering states at the initial voltage (0.1 V) and 0.4, 0.8 V are calculated.

It turns out that these bias regions exhibited the minimum current and the current inflection point. As shown in Figure 6b, three Bloch states exist in the left and right electrodes in all cases, indicating the presence of 3 transport channels. However, at V_b = 0.1 V, only 1 state is delocalized and the other two states are local which imply that most of the transmission channels are blocked. When the bias increases to 0.4 V, 3 states are all delocalized, facilitating the transfer of electrons. At V_b = 0.8 V, the second state is localized; hence, this electronic transmission channel is blocked again, resulting in a current reduction. Consequently, we propose that the current in this observation could be associated to the localization of scattering states. We note that the scattering states are gradually delocalized at a small bias. Then, the scattering states localize again and thus NDR occurs.

In general, lower adsorption energy means higher sensitivity and shorter sensing response time. Here, we revisit the results mentioned above that have shown the adsorption energy of ammonia adsorbed on $Ti_3C_2O_2$ equals −0.42 eV. In the light of Guo et al.,[39,40] adsorption smaller than −0.5 eV could facilitate the solid capture of the gas more efficiently on the surface. The external E-field which is a useful method to control the adsorption energy[38,41] is introduced to improve the sensing performance of $Ti_3C_2O_2$ to NH_3. To ensure that the geometric configuration of NH_3 adsorbed on the $Ti_3C_2O_2$ sheet is the most stable, here, we assign the electric field direction perpendicular to the MXene sheet. The positive (negative) direction is up (down), the electric field strength applied is from −0.5 to 0.5 V/Å, and the interval is 0.1 V/Å.

Figure 7a depicts the adsorption energy and the charge transfer amount of NH_3 adsorbed on $Ti_3C_2O_2$ under different

https://doi.org/10.1021/acsomega.2c07492
ACS Omega 2023, 8, 4261−4269

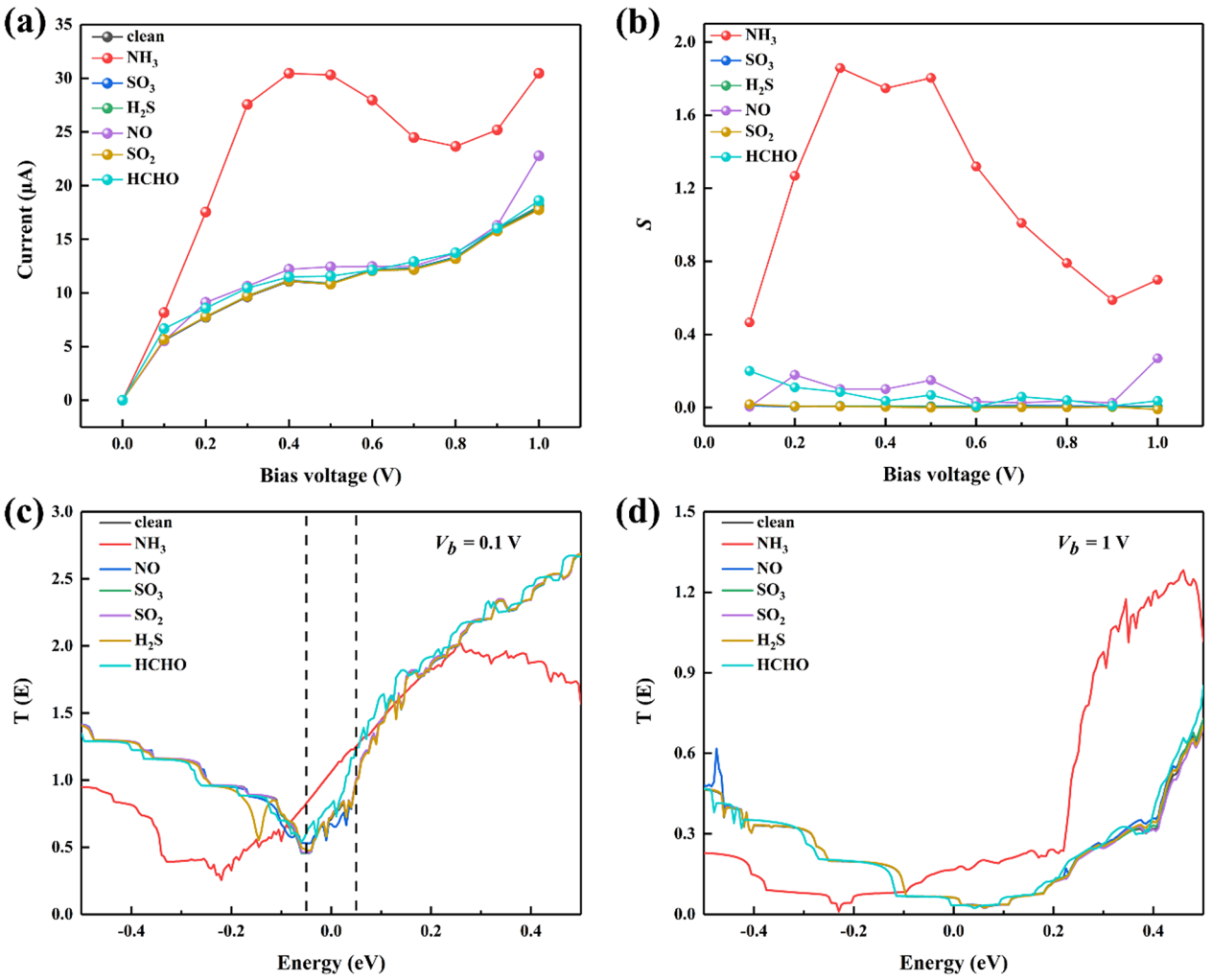

Figure 5. (a) Current−voltage (I−V) relations before and after the adsorption of the gas molecule on $Ti_3C_2O_2$, (b) sensitivity of the device to gas molecule, and transmission coefficient at (c) V_b = 0.1 V, (d) V_b = 1 V. Dashed lines represent the bias windows.

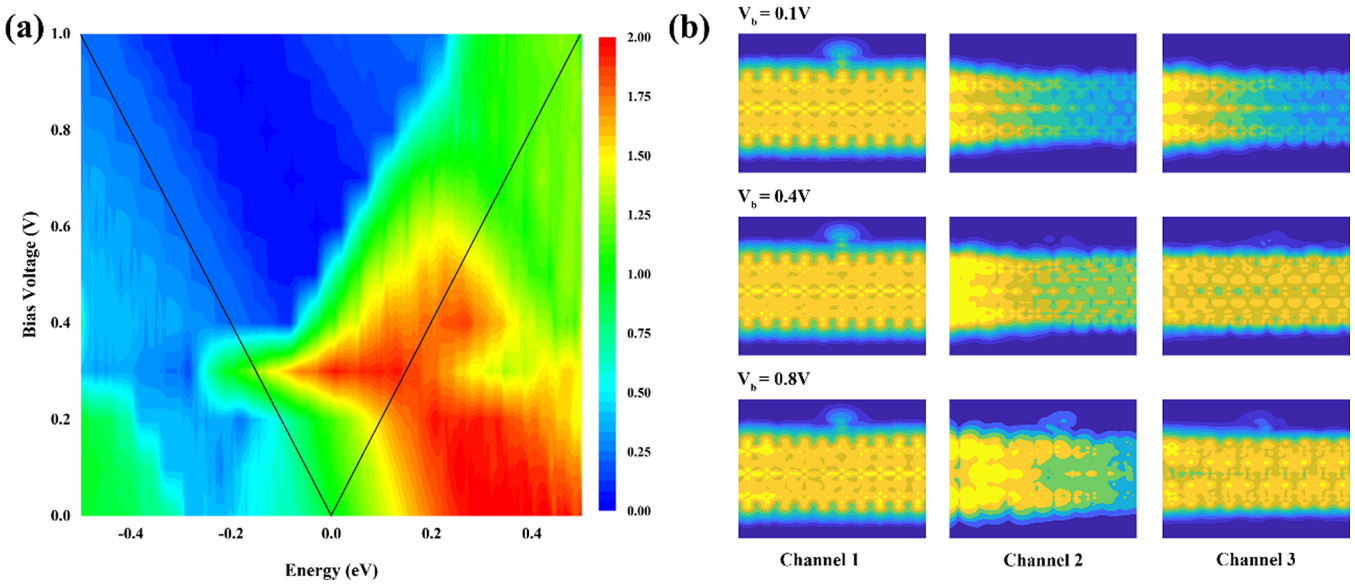

Figure 6. (a) Transmission spectra of $NH_3/Ti_3C_2O_2$ under a bias range from 0 to 1 V. Black lines represent bias windows, (b) the scattering states of $NH_3/Ti_3C_2O_2$ at V_b = 0.1, 0.4, 0.8 V, respectively.

https://doi.org/10.1021/acsomega.2c07492
ACS Omega 2023, 8, 4261−4269

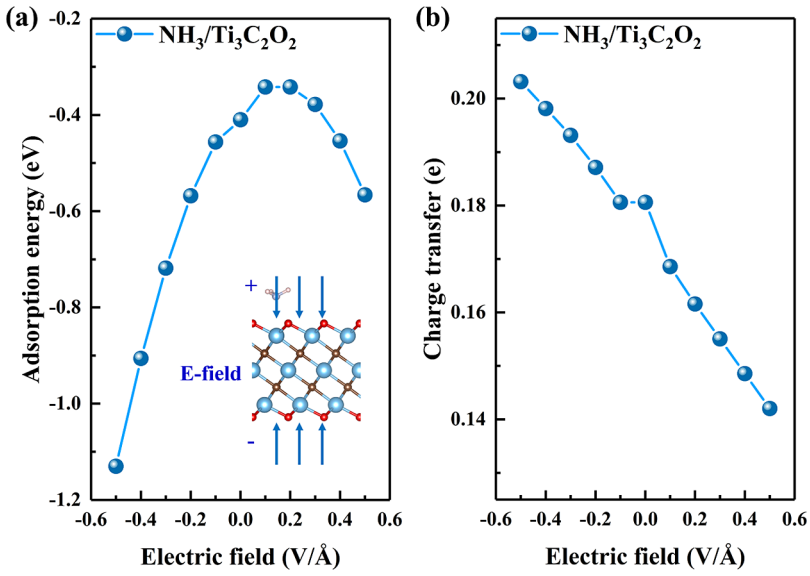

Figure 7. Electric field effects on NH_3-adsorbed $Ti_3C_2O_2$ monolayers. Variation of (a) adsorption energy and (b) charge transfer profiles.

electric fields. It is obvious that the adsorption process of NH_3 on the $Ti_3C_2O_2$ is greatly affected by the E-fields strength. When the E-fields increase negatively, as a consequence, the adsorption energy of ammonia gradually decreases. The adsorption energy can be smaller than −0.50 eV when the E-fields range from −0.5 to −0.2 V/Å. However, when the positive value of E-fields is applied, the adsorption energy of NH_3 increases first and then decreases. The largest adsorption energy achieves −0.34 eV when the E-field is 0.1 eV. The above results indicate that more effective adsorption and desorption of NH_3 can be achieved by regulating the external E-fields, which is beneficial to improve the sensing performance and facilitate the recycling of the devices.

Furthermore, we discuss the evolution of charge transfers between gases and nanosheets which is vital for sensing performance. Thus, we investigate the influence of applied electric fields on the charge transfers, as shown in Figure 7b. As the electric fields were increased from −0.5 to 0.5 V/Å, the amount of charge transfer was decreased gradually. For instance, charge transfer between NH_3 and $Ti_3C_2O_2$ could reach 0.2 e when the electric field is −0.5 V/Å, while there are 0.14 e charges transfer when the E-field is 0.5 V/Å. That is, as the E-field increases along the positive direction, the charge transfer from the gas molecule to $Ti_3C_2O_2$ decreases. The effect could be driven from to the dipole moment of NH_3 and $Ti_3C_2O_2$ and the electronegativity among H, N, Ti, C, and O atoms.[42,43] Considering that NH_3 molecules have permanent dipoles, whereas $Ti_3C_2O_2$ nanosheets have net dipole moments in zero fields, the dipole changes induced by the electric field could influence the interaction between the gas molecules and the nanosheets.

CONCLUSIONS

In summary, we investigated the physical interactions between $Ti_3C_2O_2$ and several toxic gases to elucidate their electronic structures and transport properties by DFT and NEGF. The results have shown that $Ti_3C_2O_2$ has a great promise for NH_3-sensing materials. The calculated adsorption energy of NH_3 on $Ti_3C_2O_2$ yields an appropriate value (−0.42 eV), and the charge transfer rate of 0.18 e. Then, the PDOS and charge difference density were calculated to analyze the nature of the bond between gas molecules and $Ti_3C_2O_2$.

It turns out that NH_3 molecules chemisorb on the surface and thereby trigger a substantial electronic structure variation. Although NDR appeared when NH_3 was absorbed on $Ti_3C_2O_2$, the sensitivity of $Ti_3C_2O_2$ to NH_3 was always higher than 0.4 and NH_3 showed the highest current amount of all the tested gases. The sensing performance under bias voltages ranging from 0 to 1 V revealed $Ti_3C_2O_2$-enabled stable and reliable sensing of NH_3 with small power consumption. Transmission coefficient spectra and the scattering states under different bias voltages were used to explain the reason for the emergence of NDR from the displacements of the transmission peak and the local degree of the transport channels. The adsorption energy and charge transfer upon applying external electric fields could be tuned effectively, and this facilitated the gas detection and the device recovery. Generally, $Ti_3C_2O_2$ is a promising sensing material for ammonia, and this work paves the way for designing high-yield, low-power, and high-selectivity gas sensors.

ASSOCIATED CONTENT

Supporting Information

The Supporting Information is available free of charge at https://pubs.acs.org/doi/10.1021/acsomega.2c07492.

Bader charge and adsorption energy of $Ti_3C_2T_x$; convergence test of the device potential; schematic diagram of adsorption sites; and charge transfer amount of gas molecules (PDF)

AUTHOR INFORMATION

Corresponding Author

Neng Li − *State Key Laboratory of Silicate Materials for Architectures, School of Materials and Engineering, Wuhan University of Technology, Wuhan 430070, China; Shenzhen Research Institute of Wuhan University of Technology, Shenzhen 518000 Guangdong, China; State Center for International Cooperation on Designer Low-Carbon & Environmental Materials (CDLCEM), School of Materials Science and Engineering, Zhengzhou University, Zhengzhou*

https://doi.org/10.1021/acsomega.2c07492
ACS Omega 2023, 8, 4261−4269

450001 Henan, China; orcid.org/0000-0001-9633-6702; Email: lineng@whut.edu.cn

Authors

Kaiyi Weng − *State Key Laboratory of Silicate Materials for Architectures, School of Materials and Engineering, Wuhan University of Technology, Wuhan 430070, China; Shenzhen Research Institute of Wuhan University of Technology, Shenzhen 518000 Guangdong, China*

Jiahe Peng − *State Key Laboratory of Silicate Materials for Architectures, School of Materials and Engineering, Wuhan University of Technology, Wuhan 430070, China; Shenzhen Research Institute of Wuhan University of Technology, Shenzhen 518000 Guangdong, China*

Zuhao Shi − *State Key Laboratory of Silicate Materials for Architectures, School of Materials and Engineering, Wuhan University of Technology, Wuhan 430070, China; Shenzhen Research Institute of Wuhan University of Technology, Shenzhen 518000 Guangdong, China*

Arramel Arramel − *Nano Center Indonesia, Jalan Raya PUSPIPTEK, South Tangerang, Banten 15314, Indonesia*

Complete contact information is available at: https://pubs.acs.org/10.1021/acsomega.2c07492

Notes

The authors declare no competing financial interest.

■ ACKNOWLEDGMENTS

We gratefully acknowledge HZWTECH for providing computation facilities and technical communication support. This work was supported by the Natural Science Fund for Distinguished Young Scholars of Hubei Province (No. 2020CFA087), Basic and Applied Basic Research Foundation of Guangdong Province (No. 2022A1515011303), the Basic Research Program of Shenzhen (No. JCYJ20190809120015163), the Central Government Guides Local Science and Technology Development Funds to Freely Explore Basic Research Projects (2021Szvup106), and the Fundamental Research Funds for the Central Universities (No. WUT35401053-2022).

■ REFERENCES

(1) Yamazoe, N. Toward Innovations of Gas Sensor Technology. *Sens. Actuators, B* **2005**, *108*, 2−14.

(2) Xu, Q.; Liu, Y.; Su, R.; Cai, L.; Li, B.; Zhang, Y.; Zhang, L.; Wang, Y.; Wang, Y.; Li, N.; Gong, X.; Gu, Z.; Chen, Y.; Tan, Y.; Dong, C.; Sreeprasad, T. S. Highly Fluorescent Zn-Doped Carbon Dots as Fenton Reaction-Based Bio-Sensors: An Integrative Experimental−Theoretical Consideration. *Nanoscale* **2016**, *8*, 17919−17927.

(3) Zou, J.; Mao, D.; Arramel; Li, N.; Jiang, J. Reliable and Selective Lead-Ion Sensor of Sulfur-Doped Graphitic Carbon Nitride Nanoflakes. *Appl. Surf. Sci.* **2020**, *506*, No. 144672.

(4) Imawan, C.; Solzbacher, F.; Steffes, H.; Obermeier, E. Gas-Sensing Characteristics of Modified-MoO_3 Thin Films Using Ti-Overlayers for NH_3 Gas Sensors. *Sens. Actuators, B* **2000**, *64*, 193−197.

(5) Aslam, M.; Chaudhary, V. A.; Mulla, I. S.; Sainkar, S. R.; Mandale, A. B.; Belhekar, A. A.; Vijayamohanan, K. A Highly Selective Ammonia Gas Sensor Using Surface-Ruthenated Zinc Oxide. *Sens. Actuators, A* **1999**, *75*, 162−167.

(6) Thai, N. X.; Van Duy, N.; Van Toan, N.; Hung, C. M.; Van Hieu, N.; Hoa, N. D. Effective Monitoring and Classification of Hydrogen and Ammonia Gases with a Bilayer Pt/SnO_2 Thin Film Sensor. *Int. J. Hydrogen Energy* **2020**, *45*, 2418−2428.

(7) Xu, K.; Li, N.; Zeng, D.; Tian, S.; Zhang, S.; Hu, D.; Xie, C. Interface Bonds Determined Gas-Sensing of SnO_2−SnS_2 Hybrids to Ammonia at Room Temperature. *ACS Appl. Mater. Interfaces* **2015**, *7*, 11359−11368.

(8) Gilbertson, L. M.; Busnaina, A. A.; Isaacs, J. A.; Zimmerman, J. B.; Eckelman, M. J. Life Cycle Impacts and Benefits of a Carbon Nanotube-Enabled Chemical Gas Sensor. *Environ. Sci. Technol.* **2014**, *48*, 11360.

(9) Jung, H. Y.; Kim, Y. L.; Park, S.; Datar, A.; Lee, H.; Huang, J.; Somu, S.; Busnaina, A.; Jung, Y. J.; Kwon, Y. High-Performance H_2S Detection by Redox Reactions in Semiconducting Carbon Nanotube-Based Devices. *Analyst* **2013**, *138*, 7206.

(10) Li, Y.; Zheng, Y.; Pionteck, J.; Pötschke, P.; Voit, B. Tuning the Structure and Performance of Bulk and Porous Vapor Sensors Based on Co-Continuous Carbon Nanotube-Filled Blends of Poly(Vinylidene Fluoride) and Polycarbonates by Varying Melt Viscosity. *ACS Appl. Mater. Interfaces* **2020**, *12*, 45404−45419.

(11) Virji, S.; Huang, J.; Kaner, R. B.; Weiller, B. H. Polyaniline Nanofiber Gas Sensors: Examination of Response Mechanisms. *Nano Lett.* **2004**, *4*, 491−496.

(12) Mutschall, D.; Holzner, K.; Obermeier, E. Sputtered Molybdenum Oxide Thin Films for NH3 Detection. *Sens. Actuators, B* **1996**, *36*, 320−324.

(13) Yang, S.; Jiang, C.; Wei, S. Gas Sensing in 2D Materials. *Appl. Phys. Rev.* **2017**, *4*, No. 021304.

(14) Zou, J.; Wu, J.; Wang, Y.; Deng, F.; Jiang, J.; Zhang, Y.; Liu, S.; Li, N.; Zhang, H.; Yu, J.; Zhai, T.; Alshareef, H. N. Additive-Mediated Intercalation and Surface Modification of MXenes. *Chem. Soc. Rev.* **2022**, *51*, 2972−2990.

(15) Hu, M.; Cheng, R.; Li, Z.; Hu, T.; Zhang, H.; Shi, C.; Yang, J.; Cui, C.; Zhang, C.; Wang, H.; Fan, B.; Wang, X.; Yang, Q.-H. Interlayer Engineering of $Ti_3C_2T_x$ MXenes towards High Capacitance Supercapacitors. *Nanoscale* **2020**, *12*, 763−771.

(16) Wen, Y.; Rufford, T.; Chen, X.; Li, N.; Lyu, M.; Dai, L.; Wang, L. Nitrogen-Doped $Ti_3C_2T_x$ MXene Electrodes for High-Performance Supercapacitors. *Nano Energy* **2017**, *38*, 368.

(17) Ma, R.; Chen, Z.; Zhao, D.; Zhang, X.; Zhuo, J.; Yin, Y.; Wang, X.; Yang, G.; Yi, F. $Ti_3C_2T_x$ MXene for Electrode Materials of Supercapacitors. *J. Mater. Chem. A* **2021**, *9*, 11501−11529.

(18) Zhang, Y.; Zhou, Z.; Lan, J.; Zhang, P. Prediction of $Ti_3C_2O_2$ MXene as an Effective Capturer of Formaldehyde. *Appl. Surf. Sci.* **2019**, *469*, 770−774.

(19) Qian, X.; Ma, C.; Shahid, U. B.; Sun, M.; Zhang, X.; Tian, J.; Shao, M. Synergistic Enhancement of Electrocatalytic Nitrogen Reduction over Few-Layer $MoSe_2$-Decorated $Ti_3C_2T_x$ MXene. *ACS Catal.* **2022**, *12*, 6385−6393.

(20) Sun, Y.; Jin, D.; Sun, Y.; Meng, X.; Gao, Y.; Dall'Agnese, Y.; Chen, G.; Wang, X.-F. g-C_3N_4/$Ti_3C_2T_x$ (MXenes) Composite with Oxidized Surface Groups for Efficient Photocatalytic Hydrogen Evolution. *J. Mater. Chem. A* **2018**, *6*, 9124−9131.

(21) Ebrahimi, M.; Mei, C.-T. Optoelectronic Properties of $Ti_3C_2T_x$ MXene Transparent Conductive Electrodes: Microwave Synthesis of Parent MAX Phase. *Ceram. Int.* **2020**, *46*, 28114−28119.

(22) Chen, K.; Cai, P.; Peng, H.; Xue, X.; Wang, Z.; Sun, L. $Ti_3C_2T_x$ MXene for Organic/Perovskite Optoelectronic Devices. *J. Cent. South Univ.* **2021**, *28*, 3935−3958.

(23) Ding, L.; Li, L.; Liu, Y.; Wu, Y.; Lu, Z.; Deng, J.; Wei, Y.; Caro, J.; Wang, H. Effective Ion Sieving with $Ti_3C_2T_x$ MXene Membranes for Production of Drinking Water from Seawater. *Nat. Sustainability* **2020**, *3*, 296−302.

(24) Wang, J.; Zhang, Z.; Zhu, J.; Tian, M.; Zheng, S.; Wang, F.; Wang, X.; Wang, L. Ion Sieving by a Two-Dimensional $Ti_3C_2T_x$ Alginate Lamellar Membrane with Stable Interlayer Spacing. *Nat. Commun.* **2020**, *11*, 3540.

(25) Wu, M.; He, M.; Hu, Q.; Wu, Q.; Sun, G.; Xie, L.; Zhang, Z.; Zhu, Z.; Zhou, A. Ti_3C_2 MXene-Based Sensors with High Selectivity for NH_3 Detection at Room Temperature. *ACS Sens.* **2019**, *4*, 2763−2770.

(26) Kim, S. J.; Koh, H.-J.; Ren, C. E.; Kwon, O.; Maleski, K.; Cho, S.-Y.; Anasori, B.; Kim, C.-K.; Choi, Y.-K.; Kim, J.; Gogotsi, Y.; Jung, H.-T. Metallic $Ti_3C_2T_x$ MXene Gas Sensors with Ultrahigh Signal-to-Noise Ratio. *ACS Nano* **2018**, *12*, 986−993.
(27) Kresse, G.; Furthmüller, J. Efficient Iterative Schemes for Ab Initio Total-Energy Calculations Using a Plane-Wave Basis Set. *Phys. Rev. B* **1996**, *54*, 11169−11186.
(28) Kresse, G.; Joubert, D. From Ultrasoft Pseudopotentials to the Projector Augmented-Wave Method. *Phys. Rev. B* **1999**, *59*, 1758−1775.
(29) Grimme, S.; Antony, J.; Ehrlich, S.; Krieg, H. A Consistent and Accurate *Ab Initio* Parametrization of Density Functional Dispersion Correction (DFT-D) for the 94 Elements H-Pu. *J. Chem. Phys.* **2010**, *132*, No. 154104.
(30) Taylor, J.; Guo, H.; Wang, J. Ab Initio Modeling of Quantum Transport Properties of Molecular Electronic Devices. *Phys. Rev. B* **2001**, *63*, No. 245407.
(31) Büttiker, M.; Imry, Y.; Landauer, R.; Pinhas, S. Generalized Many-Channel Conductance Formula with Application to Small Rings. *Phys. Rev. B* **1985**, *31*, 6207−6215.
(32) Ayesh, A. I.; Abu-Hani, A. F. S.; Mahmoud, S. T.; Haik, Y. Selective H_2S Sensor Based on CuO Nanoparticles Embedded in Organic Membranes. *Sens. Actuators, B* **2016**, *231*, 593−600.
(33) Tang, Q.; Zhou, Z.; Shen, P. Are MXenes Promising Anode Materials for Li Ion Batteries? Computational Studies on Electronic Properties and Li Storage Capability of Ti_3C_2 and $Ti_3C_2X_2$ (X = F, OH) Monolayer. *J. Am. Chem. Soc.* **2012**, *134*, 16909−16916.
(34) Li, L. Lattice Dynamics and Electronic Structures of $Ti_3C_2O_2$ and $Mo_2TiC_2O_2$ (MXenes): The Effect of Mo Substitution. *Comput. Mater. Sci.* **2016**, *124*, 8−14.
(35) Jayan, R.; Islam, M. M. Functionalized MXenes as Effective Polyselenide Immobilizers for Lithium−Selenium Batteries: A Density Functional Theory (DFT) Study. *Nanoscale* **2020**, *12*, 14087−14095.
(36) Abdulkader Tawfik, S.; Cui, X. Y.; Carter, D. J.; Ringer, S. P.; Stampfl, C. Sensing Sulfur-Containing Gases Using Titanium and Tin Decorated Zigzag Graphene Nanoribbons from First-Principles. *Phys. Chem. Chem. Phys.* **2015**, *17*, 6925−6932.
(37) He, C.; Zhang, M.; Li, T. T.; Zhang, W. X. Electric Field-Modulated High Sensitivity and Selectivity for NH_3 on α-C_2N_2 Nanosheet: Insights from DFT Calculations. *Appl. Surf. Sci.* **2020**, *505*, No. 144619.
(38) Ma, S.; Yuan, D.; Jiao, Z.; Wang, T.; Dai, X. Monolayer Sc_2CO_2: A Promising Candidate as a SO_2 Gas Sensor or Capturer. *J. Phys. Chem. C* **2017**, *121*, 24077−24084.
(39) Guo, H.; Zhang, W.; Lu, N.; Zhuo, Z.; Zeng, X. C.; Wu, X.; Yang, J. CO_2 Capture on *h*-BN Sheet with High Selectivity Controlled by External Electric Field. *J. Phys. Chem. C* **2015**, *119*, 6912−6917.
(40) Yu, X.; Li, Y.; Cheng, J.; Liu, Z.; Li, Q.; Li, W.; Yang, X.; Xiao, B. Monolayer Ti_2CO_2 : A Promising Candidate for NH_3 Sensor or Capturer with High Sensitivity and Selectivity. *ACS Appl. Mater. Interfaces* **2015**, *7*, 13707−13713.
(41) Wu, Y.; Chen, X.; Weng, K.; Arramel; Jiang, J.; Ong, W.; Zhang, P.; Zhao, X.; Li, N. Highly Sensitive and Selective Gas Sensor Using Heteroatom Doping Graphdiyne: A DFT Study. *Adv. Electron. Mater.* **2021**, *7*, No. 2001244.
(42) Tang, S.; Cao, Z. Adsorption of Nitrogen Oxides on Graphene and Graphene Oxides: Insights from Density Functional Calculations. *J. Chem. Phys.* **2011**, *134*, No. 044710.
(43) Li, L. Effects of the Interlayer Interaction and Electric Field on the Band Gap of Polar Bilayers: A Case Study of Sc_2CO_2. *J. Phys. Chem. C* **2016**, *120*, 24857−24865.

https://doi.org/10.1021/acsomega.2c07492
ACS Omega 2023, 8, 4261−4269